

1 Full Title: Multiscale Modeling of Superior Cavopulmonary Circulation: Hemi-Fontan
2 And Bidirectional Glenn Are Equivalent

3 Authors: Ethan Kung¹; Chiara Corsini²; Alison Marsden³; Irene Vignon-Clementel⁴;
4 Giancarlo Pennati²; Richard Figliola^{1,*}, and Tain-Yen Hsia^{5,*}; for the
5 Modeling of Congenital Hearts Alliance (MOCHA)+ Investigators

6 Affiliations:

- 7 1. Clemson University, Clemson, SC, USA,
- 8 2. Politecnico di Milano, Milan, Italy
- 9 3. Stanford University, Stanford, CA
- 10 4. National Institute for Research in Computer Science and Automation
11 (INRIA), Paris, France
- 12 5. Yale New Haven Children's Hospital, New Haven, CT

13
14 § co-first authors

15 * co-senior authors

16
17 **MOCHA Investigators:** Andrew Taylor, Sachin Khambadkone, Silvia Schievano, and
18 Marc de Leval (Institute of Cardiovascular Sciences, London, UK); Edward Bove, and
19 Adam Dorfman, (University of Michigan, Ann Arbor, MI); G. Hamilton Baker and Anthony
20 Hlavacek (Medical University of South Carolina, Charleston, SC); Francesco
21 Migliavacca, Giancarlo Pennati, and Gabriele Dubini (Politecnico di Milano, Milan, Italy);
22 Alison Marsden, (Stanford University, CA); Irene Vignon-Clementel (National Institute of
23 Research in Informatics and Automation, Paris, France); Richard Figliola and John
24 McGregor (Clemson University, Clemson, SC); Tain-Yen Hsia (Yale University, New
25 Haven, CT)

26
27 Total word count: 5924

28
29 **Funding and Conflicts of Interest:**

30 This work received funding support from Leducq Foundation (France), National Institute
31 of Health Research (UK), Burroughs Wellcome Fund (UK), American Heart Association
32 (US), National Science Foundation (US) and British Heart Foundation (UK). All authors
33 have nothing to disclose regarding possible conflicts of interest.
34

35 Corresponding Author:

36 T-Y Hsia, MD
37 Pediatric Cardiac Surgery
38 Yale New Haven Children's Hospital
39 LCCI 301, 330 Cedar Street
40 New Haven, CT, USA
41 Telephone: 1 (203) 737-1298
42 Email: tain-yen.hsia@yale.edu

Glossary

43		
44		
45	Abbreviations	
46	$art_{sat-pre}$	preoperative arterial oxygen saturation
47	$art_{sat-post}$	post-operative arterial oxygen saturation
48	bG	bi-directional Glenn
49	BSA	body surface area
50	CFD	computational fluid dynamics
51	CI	cardiac index
52	CMR	cardiac magnetic resonance imaging
53	CS	central shunt
54	GA	general anaesthetic
55	Hb	hemoglobin
56	hF	hemi-Fontan
57	HLHS	hypoplastic left heart syndrome
58	IVC	inferior vena cava
59	LPA	left pulmonary artery
60	LPN	lumped parameter network
61	$maxO_2cap$	maximum oxygen capacity
62	mBTS	modified Blalock-Taussig shunt
63	O_2del	systemic oxygen delivery
64	O_2cons	oxygen consumption
65	PA	pulmonary arteries
66	PAP	pulmonary artery pressure
67	PVR	pulmonary vascular resistance
68	$PV_{sat-pre}$	pre-operative pulmonary venous oxygen saturation
69	Q_p	pulmonary blood flow rate
70	Q_{p-pre}	pre-operative pulmonary blood flow rate
71	Q_s	systemic blood flow rate
72	SVC	superior vena cava
73	SCPC	superior cavopulmonary connection/circulation

74	TPG	transpulmonary gradient
75	3D	three-dimensional

Abstract

76
77 **Objective:** Superior cavopulmonary circulation (SCPC) can be achieved by either the
78 Hemi-Fontan (hF) or Bidirectional Glenn (bG) connection. Debate remains as to which
79 results in best hemodynamic results. Adopting patient-specific multiscale computational
80 modeling, we examined both the local dynamics and global physiology to determine if
81 surgical choice can lead to different hemodynamic outcomes.

82 **Methods:** Six patients (age: 3-6 months) underwent cardiac magnetic resonance
83 imaging and catheterization prior to SCPC surgery. For each patient: 1) a finite 3-
84 dimensional (3D) volume model of the *preoperative* anatomy were constructed to
85 include detailed definition of the distal branch pulmonary arteries, 2) virtual hF and bG
86 operations were performed to create *two* SCPC 3D models, and 3) a specific lumped
87 network representing each patient's entire cardiovascular circulation was developed
88 from clinical data. Using a previously validated multiscale algorithm that couples the 3D
89 models with lumped network, both local flow dynamics, i.e. power loss, and global
90 systemic physiology can be quantified. In two patients whose preoperative imaging
91 demonstrated significant left pulmonary artery (LPA) stenosis, we performed virtual
92 pulmonary arterioplasty to assess its effect.

93 **Results:** In one patient, the hF model showed higher power loss (107%) than the bG,
94 while in 3 the power losses were higher in the bG models (18 to 35%). In the remaining
95 two patients, the power loss differences were minor. Despite these variations, for all
96 patients, there were no significant differences between the hF and bG models in
97 hemodynamic or physiologic outcomes, including cardiac output, superior vena cava
98 pressure, right-left pulmonary flow distribution, and systemic oxygen delivery. In the two
99 patients with LPA stenosis, arterioplasty led to better LPA flow (5-8%) while halving the
100 power loss, but without important improvements in SVC pressure or cardiac output.

101 **Conclusion:** Despite power loss differences, both hF and bG result in similar SCPC
102 hemodynamics and physiology outcome. This suggests that for SCPC, the pre-existing
103 patient-specific physiology and condition, such as pulmonary vascular resistance, are

104 more deterministic in the hemodynamic performance than the type of surgical palliation.
105 Multiscale modeling can be a decision assist tool to assess whether an extensive LPA
106 reconstruction is needed at the time of SCPC for LPA stenosis.

107 (Word count = 359)

108

109

Perspective Statement

110

111 Whether hemi-Fontan or bidirectional Glenn achieves a better superior cavopulmonary
112 circulation remains debatable. Mathematical modelling incorporating both the 3D
113 anatomic detail and systemic physiology can elucidated effects of surgery in a patient
114 specific manner. We applied state of the art computational methods to demonstrate that
115 either palliation led to equivalent hemodynamic outcomes, despite differences in local
116 power loss.

117 Word count: 58 (379 characters)

118

119

Central Message

120

121 Advanced modeling simulation showed that the hemi-Fontan and bidirectional Glenn
122 achieves early equivalent superior cavopulmonary circulation hemodynamics and
123 physiology.

124

125 Word-count: 18 (163 characters)

126

127

128

129

Introduction

130
131
132 Superior cavopulmonary connection (SCPC) is a transitional circulation that allows for
133 volume off-loading of the single ventricle while providing a stable source of pulmonary
134 blood flow that can grow with the patient prior to completing single ventricle palliation
135 with a Fontan procedure. Pioneered by William Glenn at Yale in the 1960's, the classic
136 unidirectional Glenn anastomosis has been replaced by either the bidirectional Glenn
137 (bG) or the hemi-Fontan (hF) procedures. While a hF facilitates Fontan completion with
138 a lateral tunnel total cavopulmonary connection (TCPC), bG permits creation of an
139 extracardiac TCPC without the need for cardioplegic cardiac arrest. Nonetheless, the
140 choice between the adaptation of either the bG or hF to achieve SCPC remains primarily
141 based on surgeon or institutional preferences. Whereas no direct, randomized
142 comparative study has been performed to demonstrate outcome differences between
143 the two SCPC procedures, the question regarding whether one is superior than the
144 other remains unanswered with two opposing modeling studies highlighting superiority
145 of one versus the other.^{1,2}

146
147 While methodologically accurate, both of the previous computational modeling
148 investigations focused solely on the *local* flow dynamics, i.e. the flow and pressures *at*
149 the bG or hF connection. And in so doing, both studies relied on local flow dynamic
150 variables, such as power loss and flow split between the branch pulmonary arteries, to
151 assess performance differences between the bG and hF circulations. However,
152 because the SCPC is just one segment of the global cardiovascular system that is
153 composed of a closed circulatory loop, isolated SCPC modeling with open ended
154 boundary conditions cannot reveal the influence of either the bG or hF on the overall
155 systemic physiology such as SVC pressure, cardiac output, and systemic oxygen
156 delivery.

157
158 Multi-scale modeling combines the strengths of 3D computational fluid dynamics (CFD)
159 with 0-D lumped parameter network to allow comprehensive assessment of
160 hemodynamic effects of the local surgical domain and the global impact on the systemic

161 physiology. Over the last decade, we have used these validated multi-scale models to
162 evaluate a variety of clinically significant issues and concepts in patients with single
163 ventricle physiology, such as the hybrid procedure for HLHS, branch pulmonary artery
164 stenosis, residual coarctation, systemic-to-pulmonary shunts, exercise physiology,
165 cardiac biomechanics, and alternative initial palliation, and virtual surgery.³⁻⁶

166
167 In this study, we conducted an intensive mathematical modeling investigation using
168 clinical data obtained from a cohort of six patients with single ventricle hearts
169 undergoing SCPC procedure to uncover whether the choice between bG and hF
170 procedures leads to hemodynamic and physiological differences. In addition to the
171 employment of the multi-scale modeling scheme with a closed-loop cardiovascular
172 circulation, other novel concepts in this study include: 1) adaptation of *patient-specific*
173 anatomy (with detailed distal branch pulmonary arteries) and physiologic parameters
174 into the models, 2) performing virtual bG and hF procedures based on preoperative
175 magnetic resonance imaging, 3) examining the effects of relieving *patient-specific*
176 discrete left pulmonary artery (LPA) stenosis at the time of SCPC procedure, and 4)
177 quantifying both hemodynamic and physiologic variables in the context of SCPC.

Methods

178

179 Patient Selection and Clinical Data

180 Six patients (age: 3-6 month, BSA: 0.26-0.34 m²) with single ventricle cardiac defects
181 were enrolled prior to their pre-operative clinical investigations prior to their SCPC
182 procedure. Patients A, E, and F were recruited at the University of Michigan, B and D at
183 the Medical University of South Carolina, and patient C at Great Ormond Street Hospital
184 for Children (GOSH). Institutional review board study approval was obtained for each
185 clinical site and informed consent for the use of clinical data was gained from the
186 participants' legal guardians. The pre-operative clinical details of the six patients are
187 reported in Table 1. Four patients had hypoplastic left heart syndrome (HLHS) and two
188 had a hypoplastic right ventricle. At the stage 1 surgery, patient A received a 3.5mm
189 right modified Blalock-Taussig shunt (mBTS), patients B,C,E,F underwent Norwood
190 procedure with 3.5mm right mBTS, and patient D had a 4mm mBTS with left pulmonary
191 arterioplasty.

192 All patient underwent pre-operative cardiac magnetic resonance imaging (CMR), cardiac
193 catheterization and echocardiography prior to surgery. Depending on institutional
194 preferences, CMR was either performed immediately prior to surgery under the same
195 general anesthesia (GA), on the day of cardiac catheterization under the same GA with
196 transfer between imaging suites, or in a hybrid CMR catheterization imaging suite. CMR
197 was performed on 1.5T scanners (Philips Intera Achieva, Best, Netherlands; Siemens
198 Avanto, Siemens Medical Solutions, Erlangen, Germany). Contrast enhanced CMR
199 angiography was performed to obtain three-dimensional (3D) anatomical imaging with a
200 routine clinical sequence using 0.2mmol/kg of intravenous gadoteridol (Prohance;
201 Bracco Diagnostics, Princeton, NJ). Free-breathing, electrocardiogram-gated velocity-
202 encoded phase contrast imaging sequences were used to acquire flow measurements in
203 the ascending and descending aorta, pulmonary arteries and veins, and inferior (IVC)
204 and superior vena cavae (SVC).

205

206 Cardiac catheterization followed a routine clinical protocol under GA or sedation in a bi-
207 plane fluoroscopy suite (Siemens Medical Solutions USA, Inc. Pennsylvania). A fluid-
208 filled catheter system was used to acquire pressure traces and hemodynamic
209 measurements in the ascending and descending aorta, systemic atrium, and single
210 ventricle. Pulmonary artery pressure (PAP) was either a direct measurement or an
211 estimate from pulmonary venous wedge pressure. In patients C, E, and F, PAP was
212 acquired on the left side, with no clinical evidence suggestive of a stenosis or cause for
213 discrepancy between the two pulmonary arteries (PA). In patients A, B, and D, PAPs
214 were acquired on the left and right sides. Patient B also had left pulmonary artery
215 stenosis (PAS), and patient D had left PAS with a 3mmHg pressure difference between
216 the two pulmonary arteries. Only in patient D did the clinical team felt a left pulmonary
217 arterioplasty was indicated. Pre-operative echocardiography was performed under GA
218 or sedation. Pulsed wave Doppler traces were acquired in the aorta, SVC, IVC and
219 branch PAs.

220 All clinical data processing occurred at one core laboratory (GOSH). A representation of
221 the patients' pre-operative physiology was constructed from CMR flows and invasive
222 mean pressure measurements. The resulting parameters presented in Table 2 were
223 used to tune the multiscale models as described below. Flow measurements were
224 calculated using an in-house plug-in for OsiriX open-source software (OsiriX
225 Foundation, Geneva, Switzerland). These are reported indexed to BSA to aid
226 comparison between patients.

227 Three-dimensional (3D) models and virtual surgery

228 3D models of each patients' stage 1 anatomy were reconstructed from the CMR
229 angiographic sequences using commercially available software (Mimics, Materialise NV,
230 Leuven, Belgium). In Figure 1, we illustrate the reconstruction process using Patient B
231 as an example, while Figure 2 depicts the stage 1 and stage 2 reconstructions for the six
232 patients studied. Referring to Figure 1, a region of interest was selected within the
233 relevant area of surgical anatomy. A 3D geometrical model was constructed through a
234 process of region-growing and segmentation.^{7,8} The pre-operative 3D model for each

235 patient included the mBTS and PAs extended to the furthest branch level visible for
236 reconstruction (Figure 1, stage 1). The location of the SVC and atrium was noted for
237 construction of the stage 2 virtual surgery. To this end, the stage 1 geometry was
238 manipulated virtually, removing the mBTS and inserting the reconstructed SVC in its
239 stead, merging the volumes with a Boolean operation (Figure 1, stage 2). In the case of
240 hF, a portion of the atrium was reconstructed from the original CMR dataset and
241 similarly merged in the 3D domain, again after removal of the mBTS. In both cases,
242 where appropriate, a pulmonary arterioplasty model was generated by virtually enlarging
243 the caliber of the narrowed PA. Prior to use for stage 2 simulations, the realistic nature
244 of all virtual surgery models shown in Figure 2 was verified by the surgeons (EB, TYH)
245 involved in the study.

246

247 Multiscale Simulation and Analysis

248 Multi-scale models were developed and tuned for each patient based on the patient-
249 specific anatomical and clinical data (Table 2). According to our previous work,^{3,4} we
250 constructed a 0D LPN to model the circulatory system outside of the surgical region,
251 which was coupled directly to the inflow and outflow passages of the 3D model of the
252 surgical site. Briefly, the closed-loop LPN includes sections that describe the heart,
253 upper and lower body vasculatures, pulmonary vasculature, and vascular beds in
254 several abdominal organs. The contraction and filling of each heart chamber is
255 described via a passive and active pressure-volume curve and an activation function.^{3,4}
256 This allows the simulation to capture effects of preload on cardiac output due to the
257 Frank-Starling mechanism. The influence of respiration was neglected for this study.

258

259 Each patient was modeled at the age and body surface area (BSA) at the time of their
260 CMR scan since both 3D and flow information is acquired at this time-point. As
261 described in our prior work, most elements of the LPN were tuned initially using
262 reference values (that were scaled by allometric equations based on each patient's
263 particular BSA and then further adjusted for each patient based on available clinical
264 data.⁹⁻¹² The LPN parameters in the pulmonary vasculature were automatically

265 estimated based on multiscale preoperative simulations to match the relevant clinical
266 measurements.¹³ We divided the pulmonary vasculature into several parts to be
267 represented as lumped components. These parts include the large arteries, smaller
268 arteries, capillaries, and veins; Next, empirical laws determined the distribution of the
269 equivalent resistance and capacitance over the arterial or venous sides.¹⁴⁻¹⁶
270 Windkessel models were generated from the Womersley-based impedance of each
271 pulmonary branch,^{17,18} therefore the proximal to distal pulmonary artery resistance ratio
272 is different for each branch. Combining all of these relations provided a unique set of
273 LPN parameters for each pulmonary branch based on its total resistance.

274 Multi-scale simulations of the post-operative scenarios were conducted according to
275 previously validated techniques.^{7, 12, 19, 20} Briefly, this involves discretizing the 3D virtual
276 surgery geometries into isotropic finite-element meshes with maximum edge size of 0.03
277 cm (MESHSIM, Simmetrix Inc., New York) and coupling the 3D Navier-Stokes equations
278 to the 0D LPN using Neumann boundary conditions, implicit coupling, and outflow
279 stabilization.²¹ Flow and pressure in the 3D and LPN domain were solved using a
280 custom incompressible finite element Navier-Stokes solver (Simvascular,
281 www.simtk.org), and a 4th order Runge-Kutta algorithm, respectively. Simulation time
282 step size was 1 ms and 1 μ s for the 3D and LPN domain, respectively. Flow and
283 pressure coupling between domains occurs at every 3D time step. Each simulation
284 included 12 cardiac cycles where the last cycle data, by which periodicity had been
285 achieved, was used in the final results analysis.

286 Power loss was calculated from the simulation results according to our previous
287 publication.⁴ To summarize, the surgical junction power loss was obtained from the 3D
288 data by integrating the sum of inlet and outlet face energy fluxes, which accounts for
289 both the potential and kinetic energy. The power loss across a vascular bed was
290 obtained from the 0D data by multiplying the pressure drop and the total flow across the
291 vascular bed.

292 Post-operative predictions of systemic oxygen delivery, and arterial and venous

293 saturations were calculated using a combination of pre-operative clinical measurements
 294 and post-operative predictions of flow. We assumed: 1) the pre-operative estimates of
 295 maximum oxygen capacity and oxygen consumption remained the same immediately
 296 following surgery; 2) pulmonary venous saturations remain the same immediately post-
 297 operatively; and 3) the relative upper and lower body oxygen consumption after surgery
 298 is directly proportional to flow. The maximum oxygen carrying capacity of blood
 299 $maxO_2cap$ (mlO₂/100ml) was estimated as

$$300 \quad maxO_2cap = Hb_{pre} \times 1.34 \quad (1)$$

301 where Hb_{pre} is pre-operative hemoglobin in g/dL and 1.34 represents Hüfner's constant
 302 (a directly measured estimate of the maximum oxygen carrying capacity of blood equal
 303 to 1.34ml O₂/g of hemoglobin). The oxygen consumption O_2cons (mlO₂/min/m²) was
 304 estimated as

$$305 \quad O_2cons = Q_{p-pre} \times \frac{PV_{sat-pre} - art_{sat-pre}}{100} \times maxO_2cap \times 10 / BSA \quad (2)$$

306 where Q_{p-pre} is the pre-operative measured pulmonary flow (L/min), $PV_{sat-pre}$ is the
 307 measured pre-operative pulmonary venous oxygen saturations (%), $art_{sat-pre}$ is the
 308 measured arterial oxygen saturations (%), and BSA is body surface area (m²). The post-
 309 operative estimated systemic oxygen delivery O_2del (mlO₂/min/m²) was calculated as

$$310 \quad O_2del = \frac{(Q_s \times \frac{PV_{sat-pre}}{100} \times maxO_2cap \times 10) - (\alpha_{LB} \times O_2cons \times BSA)}{BSA} \quad (3)$$

311 where Q_s is systemic flow (L/min) calculated from the post-operative simulation, α_{LB} is
 312 the proportion of Q_s to the lower body based on post-operative simulation results, and
 313 Q_p is the post-operative pulmonary flow (L/min) from simulation results. The post-
 314 operative arterial oxygen saturation $art_{sat-post}$ (%) was estimated as

$$315 \quad art_{sat-post} = \frac{O_2del}{Qs} \times \frac{BSA}{\max O_2cap \times 10} \quad (4)$$

316
317

Results

318 There were significant differences in local flow patterns and pressure distributions
319 between the two surgical options. Using the results for patient B as an example (Figure
320 3), the bG geometry typically reveals a flow jet of blood from the SVC that impinges on
321 the bottom of the PA wall at the anastomosis where it divides to the branches (Figure 3,
322 A and C). However, in the hF geometry there is slight vortex of blood as the incoming
323 SVC flow glides along the atrial wall (Figure 3, B and D). In the cases where an LPA
324 stenosis is present (Figure 3, A and B), there is also a flow jet following and a nominal
325 1mmHg pressure loss across the stenosis. The pressure and flow patterns predicted
326 here were consistent with those of a previous study on patients at the same stage but
327 right before the Fontan surgery.¹⁸

328 The local power loss in the surgical SCPC junction (Table 3, 3D power loss) varied
329 considerably between bG and hF models. In four patients, hF showed a notably higher
330 power loss (18 to 107%) than bG, which was consistent with the differences in flow
331 fields and pressures between these differing surgical options. In two patients, power
332 losses were essentially equivalent (< 7% difference) between options. In comparing the
333 3D power loss with the total power loss across the entire pulmonary vascular bed (Table
334 3), the amount of power loss occurring within the SCPC junction is only 1 to 16% of that
335 across the entire pulmonary circulation. The magnitudes of these power losses are
336 compared directly in Figure 4. Much larger differences in the total pulmonary power loss
337 exist between patients with different pulmonary vascular resistances (PVR) than
338 between the different surgical options of the same patient.

339 As a consequence, the post-operative SCPC simulation results revealed similar
340 physiologic outcomes between the various surgical options for each patient (Table 3).
341 The bG and hF surgical models had small differences in transpulmonary gradient (TPG)

342 and SVC pressure (P_{SVC}) (up to 5% and 2%, respectively), and negligible differences in
343 cardiac index (CI) (<1%) with nearly identical pulmonary to systemic flow splits. Oxygen
344 delivery (Table 3) closely followed cardiac index for each patient, and both oxygen
345 delivery and oxygen saturations were insensitive to the surgical option for a specific
346 patient.

347 The power losses in models with left PAS were found to be more than two times higher
348 (217-248%) than that in models where the left PAS was relieved by virtual arterioplasty.
349 While the relief of PAS led to slightly better LPA flow (5-8%) in both patients, there was
350 no important improvement in SVC pressure or cardiac output compared to models
351 where the left PAS was left intact.

352

Discussion

353
354 In 1996, Marc de Leval and his collaborators in Milan, Italy reported the first instance
355 where computational fluid dynamics (CFD), a relatively new engineering field, was
356 applied to the evaluation of a reconstructive cardiac procedure.²⁴ While the
357 mathematics were sophisticated and investigation revealed interesting flow dynamic
358 insights in the TCPC, the problem facing the investigators was how to translate the
359 mathematical information to the surgical community. They needed a parameter or
360 variable that a congenital cardiac surgeon can appreciate its value and correlate with
361 clinical significance. Since the ability of CFD at that time only allowed for modeling an
362 isolated surgical domain, i.e. the cavopulmonary connections, their models required
363 compulsory open-ended inlets and outlets with rigid, prescribed boundary conditions.
364 And in such an open-loop circulatory model, only the local pressure and flow conditions
365 can be quantified, leaving any interaction with the rest of the global, systemic circulation
366 unanswered. Therefore, as a way to quantify the 'performance' of a cavopulmonary
367 connection, the concept of power loss was introduced to describe the *extraction* of fluid
368 dynamic power, or energy, as blood traversed from the inlets (vena cava) to the outlets
369 (branch pulmonary arteries). Less power loss in a cavopulmonary circulation, the better.
370 And power loss became the goal post for which future modeling investigations of the
371 cavopulmonary circulation would be based on. ^{1,2,18,22}

372 In this study, where a closed loop circulatory model allowed for interaction between the
373 SCPC and the rest of the cardiovascular system, our *patient-specific* multi-scale
374 simulations showed that differences in power loss between a hF and bG SCPC, even
375 when greater than two-fold, resulted in negligible effect on clinically relevant parameters
376 such as cardiac index, SVC pressure, and systemic oxygen delivery. Therefore, either
377 hF or bG, as the procedure of choice for SCPC, would achieve similar hemodynamic
378 and physiologic results. This is unlikely to be a controversial finding, as most surgeons
379 would agree that outcomes after either procedure have been viewed to be similar.
380 Nonetheless, by employing the state of art multi-scale modeling with patient-specific
381 anatomy and physiology information, this study should settle the hF versus bG debate
382 while highlighting the importance of evaluating the hemodynamic performance of a

383 cardiac surgical procedure, not in isolation, but in context of the global systemic
384 circulation.

385 So, why is power loss differences between hF and bG not important? This can be
386 explained by examining the SCPC junction power loss in the context of the systemic
387 circuit. An advantage of multi-scale computational modeling is this inclusion of the
388 patient-specific systems-level physiology on the predicted hemodynamic outcomes.
389 Due to the fact that only a small fraction of the power loss in the pulmonary circulation
390 actually occurs over the SCPC junction, change in the junction power loss by several
391 folds can still only have limited effects on the overall circulation. As noted, Figure 4
392 illustrates the contribution of the SCPC junction power loss to the *total* pulmonary power
393 loss in each patient. It is clear that much of the power loss via the pulmonary circulation
394 occurs outside of the surgical junction, meaning that the patient PVR has a much larger
395 impact on the overall physiology than the hemodynamic differences between hF and bG.
396 We observed the same relative significance between the SCPC and total pulmonary
397 power loss in all 6 patients. There is a caveat, however: this does not mean power loss
398 does not matter at all. In situations or conditions where there is important lesion that
399 impacts on blood flow, such as severe LPA stenosis or SCPC anastomotic obstruction,
400 the power loss through a cavopulmonary connection can become high enough to be on
401 similar order as PVR and there will be adverse hemodynamic consequences. Also,
402 under higher metabolic states, such as exercise, as flow increases and PVR drops, the
403 ratio between the SCPC and the total pulmonary power loss is expected to rise. Further
404 studies will be needed to determine whether this would result in more noticeable
405 differences in physiology between different surgical geometries.

406 The multi-scale simulations also revealed that in two patients with discrete left PA
407 stenosis, virtual augmentation with arterioplasty did not lead to important benefits in the
408 overall performance and hemodynamics of the SCPC. This suggests that, in these two
409 patients, a more extensive and potentially risky operation (i.e. division of the Damus-
410 Kay-Stansel anastomosis to get to the left PA) to relieve LPA stenosis would not have
411 led to additional hemodynamic and physiologic benefits. Again, this discovery cannot be

412 applied to all instances of left PA stenosis, as surely relief of severe left PA stenosis is
413 important at the time of a cavopulmonary connection procedure. Nonetheless, these
414 simulation results suggests that not all left PA stenosis requires extensive arterioplasty,
415 and a combination of virtual surgery with multi-scale modeling can provide valuable
416 support and guidance to a surgeon's decision on whether a patient-specific left PA
417 stenosis can be left untouched at the time of SCPC.

418 Closed loop modeling of stage 1 physiology represents a challenge due to the
419 complexity of the physiology and time-varying nature of the hemodynamic
420 measurements. Clinical data is acquired at different time points and used to build a
421 representation of the patient's pre-operative physiology. The aim of this study was to
422 compare the effect of different surgical anatomies, without additional adaptation from the
423 global physiology. Consequently, responses such as post-operative stress response,
424 effects of medication, chronic adaption to new ventricular loading conditions, post-
425 operative complications, and the effects of growth on the clinical data are not modeled.
426 In light of this, validation of the predicted results against existing clinical data remains
427 limited. The simulations represent a prediction of the *immediate* post-operative
428 physiology based on the physiological impacts of loading changes induced by the
429 surgical procedures only. A direct comparison between the surgical options is essential
430 for gaining a mechanistic understanding of the hemodynamics in the relevant clinical
431 scenarios. One step towards assessing the robustness of the predicted results would
432 be to incorporate approaches that also contain sensitivity analysis¹⁸ or uncertainty
433 quantification²³, including both the clinical data and physiological model parameters.
434 This might be especially important when preoperative clinical data are not coherent.¹³
435 Currently, such methods are computationally expensive and in need of further
436 development.²³ It is also important to point out that while variation in the bi-directional
437 Glenn procedure is limited, the construction of a hemi-Fontan can be quite variable from
438 one institution and one surgeon to another. As only one institution (Michigan) in our
439 collaboration routinely applied the hemi-Fontan, we have adopted virtual hemi-Fontan
440 models without additional patch enlargement of the left pulmonary artery was described
441 by William Norwood. Therefore, it is possible that an left PA stenosis will routinely be

442 addressed by this manner of hemi-Fontan construction. Finally, any virtual surgery and
443 computational modeling investigation, even using patient specific information, cannot
444 account for all the biological and clinical processes that impacts on ultimate outcome.
445 Therefore, the findings from this study should be applied in the context of clinical
446 decision-making support.

447

448 **Conclusion**

449 In this first case series of patient-specific multiscale modeling of superior cavopulmonary
450 connection palliation for single ventricle hearts, virtual hemi-Fontan and bidirectional
451 Glenn procedures were simulated based on each patient's *preoperative* anatomy and
452 physiologic conditions derived from clinically indicated investigations. Despite what
453 appeared to be significant local power loss differences, both the hemi-Fontan and
454 bidirectional Glenn procedures resulted in similar early postoperative superior
455 cavopulmonary hemodynamics and physiology. Moreover, simulations suggest that
456 multi-scale modeling may be helpful to support patient-specific decision on whether an
457 aggressive left pulmonary artery reconstruction at the time of SCPC procedure could be
458 beneficial.

Acknowledgements and Disclosures

459

460

461

462 The authors gratefully acknowledge support from Foundation Leducq.

463

464 The authors have nothing to disclose with regard to commercial support.

465

References

- 466
- 467 1. Bove EL, de Leval MR, Migliavacca F, Guadagni G, Dubini G, Computational fluid
468 dynamics in the evaluation of hemodynamic performance of cavopulmonary
469 connections after the Norwood procedure for hypoplastic left heart syndrome. *J*
470 *Thorac Cardiovasc Surg* 126, 1040-1047 (2003).
- 471 2. Pekkan K et al., Hemodynamic Performance of Stage-2 Univentricular
472 Reconstruction: Glenn vs. Hemi-Fontan Templates. *Ann Biomed Eng* 37, 50-63
473 (2009).
- 474 3. Corsini C et al., An integrated approach to patient-specific predictive modeling for
475 single ventricle heart palliation. *Comput Methods Biomech Biomed Engin*,
476 (2013).
- 477 4. Kung E et al., Predictive modeling of the virtual Hemi-Fontan operation for
478 second stage single ventricle palliation: Two patient-specific cases. *J*
479 *Biomechanics* 46, 423-429 (2013).
- 480 5. Schiavazzi DE et al., Hemodynamic effects of left pulmonary artery stenosis after
481 superior cavopulmonary connection: A patient-specific multiscale modeling study.
482 *J Thorac Cardiovasc Surg* 149, 689-696.e683 (2015).
- 483 6. Vignon-Clementel IE, Marsden AL, Feinstein JA. A primer on computational
484 simulation in congenital heart disease for the clinician. *Prog. Pediatr. Cardiol.*
485 30(1), 3–13, 2010.
- 486 7. Corsini C et al., An integrated approach to patient-specific predictive modeling for
487 single ventricle heart palliation. *Comput Methods Biomech Biomed Engin*,
488 (2013).
- 489 8. Schievano S et al., Percutaneous pulmonary valve implantation based on rapid
490 prototyping of right ventricular outflow tract and pulmonary trunk from MR data.
491 *Radiology* 242, 490-497 (2007).
- 492 9. Snyder MF, Rideout VC, 1969. Computer simulation studies of the venous
493 circulation. *IEEE Transactions on Biomedical Engineering* 16, 325–334.
- 494 10. Noordergraaf A, Verdouw D, Boom HB, 1963. The use of an analog computer in
495 a circulation model. *Progress in Cardiovascular Diseases* 5, 419–439.

- 496 11. Pennati G, Fumero R, 2000. Scaling approach to study the changes through the
497 gestation of human fetal cardiac and circulatory behaviors. *Annals of Biomedical*
498 *Engineering* 28, 442–452.
- 499 12. Kung E et al., Predictive modeling of the virtual Hemi-Fontan operation for
500 second stage single ventricle palliation: Two patient-specific cases. *J Biomech*
501 46, 423-429 (2013).
- 502 13. Arbia, G., Corsini, C., Baker, C., Pennati, G., Hsia, T.-Y., Vignon-Clementel,
503 I., 2015. Pulmonary hemodynamics simulations before stage 2 single ventricle
504 surgery: Patient-specific parameter identification and clinical data assess-
505 ment. *Cardiovascular Engineering and Technology*, 1-13.
- 506 14. Brody JS, Stemmler EJ, DuBois AB. Longitudinal distribution of vascular
507 resistance in the pulmonary arteries, capillaries, and veins. *J. Clin. Invest.* 47,
508 783–799 (1968). DOI 10.1172/JCI1105773
- 509 15. O'Leary CE, Fiori R, Hakim TS. Perioperative distribution of pulmonary vascular
510 resistance in patients undergoing coronary artery surgery. *Anesth. Analg.* 82,
511 958–963 (1996)
- 512 16. Presson RG, Audi SH, Hanger CC, Zenk GM, Sidner RA, Linehan JH, Wagner
513 WW, Dawson CA. Anatomic distribution of pulmonary vascular compliance. *J.*
514 *Appl. Physiol.* 84, 303–310 (1998)
- 515 17. Spilker RL, Feinstein JA, Parker DW, Reddy VM, Taylor CA, 2007. Morphometry-
516 based impedance boundary conditions for patient-specific modeling of blood flow
517 in pulmonary arteries. *Annals of Biomedical Engineering* 35, 546–559.
- 518 18. Troianovski G., Taylor CA, Feinstein JA, Vignon-Clementel IE. 2011. Three-
519 dimensional simulations in Glenn patients: clinically based boundary conditions,
520 hemodynamic results and sensitivity to input data. *Journal of Biomechanical*
521 *Engineering* 133, 111006.
- 522 19. Baker CE et al., Effects of pulmonary artery banding and retrograde aortic arch
523 obstruction on the hybrid palliation of hypoplastic left heart syndrome. *J Thorac*
524 *Cardiovasc Surg*, (2013).
- 525 20. Hsia TY et al., Use of mathematical modeling to compare and predict
526 hemodynamic effects between hybrid and surgical Norwood palliations for
527 hypoplastic left heart syndrome. *Circulation* 124, S204-210 (2011).
- 528 21. Esmaily Moghadam M., Bazilevs Y, Hsia TY, Vignon-Clementel IE, Marsden AL,
529 A comparison of outlet boundary treatments for prevention of backflow
530
- 531
532

- 533 divergence with relevance to blood flow simulations. *Computational Mechanics*,
534 1-15 (2011).
- 535 22. Dasi, L. P., KrishnankuttyRema, R., Kitajima, et al.. Fontan hemodynamics:
536 importance of pulmonary artery diameter. *J Thoracic Cardiovasc Surg*, 137(3),
537 560-564. (2009)
- 538 23. Schiavazzi DE, Arbia G, Baker C, Hlavacek AM, Hsia TY, Marsden AL, Vignon-
539 Clementel IE, et al. Uncertainty quantification in virtual surgery hemodynamics
540 predictions for single ventricle palliation. *International Journal for Numerical*
541 *Methods in Biomedical Engineering*, 2015.
- 542 24. de Leval MR, Dubini G, Migliavacca F, Jalali H, Camporini G, Redington A,
543 Pietrabissa R. Use of computational fluid dynamics in the design of surgical
544 procedures: application to the study of competitive flows in cavo-pulmonary
545 connections. *J Thorac Cardiovasc Surg*. 1996 Mar;111(3):502-13.
- 546

547

548

549 **List of Tables**

550 Table 1: Pre-operative demographics of the six patients used for the study.

551 Table 2: Clinical parameters used for pre-operative multiscale modeling.

552 Table 3: Post-operative predictions.

Table 1: Pre-operative demographics of the six patients used for the study

Patient	A	B	C	D	E	F
Age* (months)	6	3	4	3	4	5
BSA (m²)	0.34	0.30	0.27	0.26	0.28	0.34
Diagnosis	PA/IVS	MS, AS	MS, AS	TA, PA left PAS	MA, AA	MA, AA
Stage 1 surgery	3.5mm mBTS	Norwood 3.5mm mBTS	Norwood 3.5mm mBTS	4mm mBTS with LPAPlasty	Norwood 3.5mm mBTS	Norwood 3.5mm mBTS

*Age used for model construction

BSA: body surface area; PA/IVS: pulmonary atresia/intact ventricular septum; mBTS: modified Blalock-Taussig shunt; MS: mitral stenosis; AS: aortic stenosis; TA: tricuspid atresia, PAS: pulmonary artery stenosis; MA: mitral atresia; AA: aortic atresia

Table 2: Clinical parameters used for pre-operative multiscale modeling

Patient	A	B	C	D	E	F
CI (L/min/m ²)	4.31	4.08	6.87	6.23	5.79	5.47
Qp (L/min/m ²)	1.32	1.94	3.69	2.77	2.57	3.53
Qrpa : Qp (%)	64	46	51	67	46	55
Qp : Qs	0.44	0.91	1.16	0.80	0.80	1.81
mP_{atr} (mmHg)	5	6	6	7	5	4
mPAP (mmHg)	13(R), 12(L)	12(R/L)	11(L)	17(R), 14(L)	13 (L)	13.5(L)
TPG (mmHg)	8	6	5	10	8	9.5
mP_{Ao} (mmHg)	43 [#]	52	51	53	53	72
PVR (WU*m ²)	6.0	3.1	1.4	3.6	2.8	2.7
SVR (WU*m ²)	12.7	21.5	14.2	13.3	14.8	35.0

[#]estimated from left upper limb sphygmomanometer

CI: cardiac index; Qp and Qs: pulmonary and systemic flow; Qrpa: right pulmonary artery flow; mP_{atr}: mean systemic atrial pressure; mPAP: mean pulmonary artery pressure; R/L: right/left; TPG: transpulmonary gradient; mP_{Ao}: mean invasive ascending aortic pressure; PVR and SVR: pulmonary and systemic vascular resistance.

Table 3: SCPC simulation results

Patient	A		B				C		D				E		F	
Procedure	bG	hF*	bG	bG(ns)*	hF	hF(ns)	bG*	hF	bG	bG(ns)*	hF	hF (ns)	bG	hF*	bG	hF*
CI (L/min/m ²)	3.40	3.38	3.34	3.35	3.34	3.35	5.25	5.24	4.29	4.32	4.28	4.32	3.87	3.86	3.64	3.64
Qp (L/min/m ²)	2.01	1.99	1.63	1.64	1.63	1.64	2.88	2.87	2.66	2.70	2.65	2.69	2.74	2.73	2.58	2.58
Qrpa : Qp (%)	63	63	59	54	59	54	51	48	69	61	68	60	45.0	45.0	56	55
Qp : Qs	0.59	0.59	0.49	0.49	0.49	0.49	0.55	0.55	0.62	0.62	0.62	0.62	0.71	0.71	0.71	0.71
P _{atr} (mmHg)	2.48	2.43	4.59	4.62	4.60	4.63	5.22	5.22	4.67	4.71	4.66	4.71	3.63	3.62	2.46	2.46
P _{svc} (mmHg)	15.07	15.38	10.49	10.02	10.43	10.02	10.11	10.19	14.67	13.76	14.91	13.84	11.92	12.09	10.30	10.26
TPG (mmHg)	12.18	12.13	5.05	4.70	5.07	4.93	4.25	4.24	8.05	8.34	8.04	8.37	8.19	8.18	7.20	7.20
Ao MAP (mmHg)	53.06	53.10	74.9	74.9	74.9	74.9	80.4	80.42	67.0	66.9	67.1	66.9	65.9	65.9	131.4	131.4
3D Power loss (mW)	0.61	1.26	0.87	0.35	0.82	0.33	1.05	1.24	2.00	0.92	2.51	1.11	0.95	1.28	1.20	1.12
PA-Sa power loss (mW)	18.49	18.18	5.54	5.59	5.57	5.62	15.54	15.61	13.31	13.15	13.14	13.08	13.81	13.74	14.00	13.98
Total pulmonary power loss	19.10	19.44	6.41	5.94	6.39	5.95	16.59	16.85	15.31	14.07	15.65	14.19	14.76	15.02	15.20	15.10
SCPC : Total Pulmonary power loss (%)	3.2	6.5	13.6	5.9	12.8	5.5	6.3	7.4	13.1	6.5	16.0	7.8	6.4	8.5	7.9	7.4
Oxygen delivery (mlO ₂ /min/m ²)	597	593	599	602	602	603	1006	1005	806	812	804	812	746	746	867	867
O ₂ sat Ao	82	82	84	84	84	84	89	89	88	88	88	88	90	90	91	91

*actual surgical procedure performed

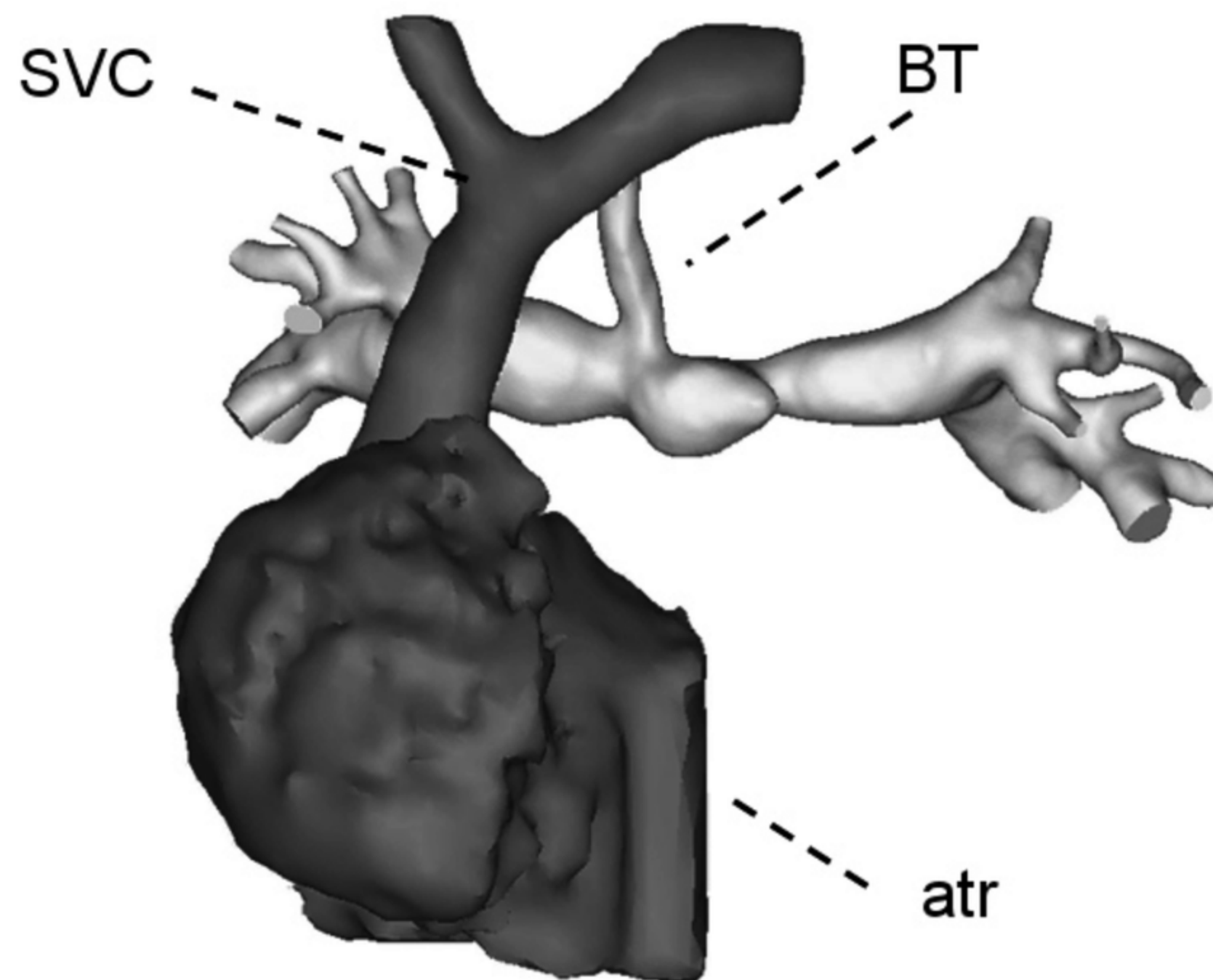
SCPC: superior cavopulmonary connection; bG: bidirectional Glenn; hF: hemi-Fontan; ns: no left PA stenosis; CI: cardiac index; Q_p and Q_s : pulmonary and systemic flow; Q_{rpa} : right pulmonary artery flow; P_{atr} : common atrial pressure; P_{svc} : superior vena cava pressure; TPG: transpulmonary gradient; Ao MAP: aortic mean arterial pressure; PA-Sa: pulmonary artery to systemic atrial; Ao: a

Figure Legends

- Figure 1. An example of the virtual bG and hF superior cavopulmonary surgeries using patient B. Top panel demonstrates the preoperative (Stage 1) anatomy obtained from MRI. Middle panel demonstrates virtual bG and hF surgeries. Bottom panel demonstrates virtual bG and hG procedures with concomitant left pulmonary arterioplasty for relieve of left pulmonary arterial stenosis. SVC: superior vena cava; BTS: Blalock-Taussig shunt; atr: atrium; bG: di-directional Glenn; hF: hemi-Fontan; PA: pulmonary artery
- Figure 2. The preoperative anatomical reconstruction (stage 1) and virtual surgery (stage 2) for all six patients studied. Patients B and D had left pulmonary arterial stenosis preoperatively, and virtual SCPC surgeries were performed with and without concomitant left pulmonary arterioplasty. bG: di-directional Glenn; hF: hemi-Fontan; PA: pulmonary artery
- Figure 3: Mid-systolic pressure and velocity maps for patient B. Panel A: bi-directional Glenn with left pulmonary artery stenosis; panel B: hemi-Fontan with left pulmonary artery stenosis; panel C: bi-directional Glenn with pulmonary arterioplasty; panel D: hemi-Fontan with pulmonary arterioplasty.
- Figure 4. A comparison of the power loss in the SCPC surgical junction and the total power loss through the pulmonary circulation. Power loss through the SCPC surgical junction, whether bG or hF, represents a very small part of the overall power loss in the superior cavopulmonary circulation. bG: di-directional Glenn; hF: hemi-Fontan; PA: pulmonary artery; ns: no pulmonary arterial stenosis; mW: milli-

Watts.

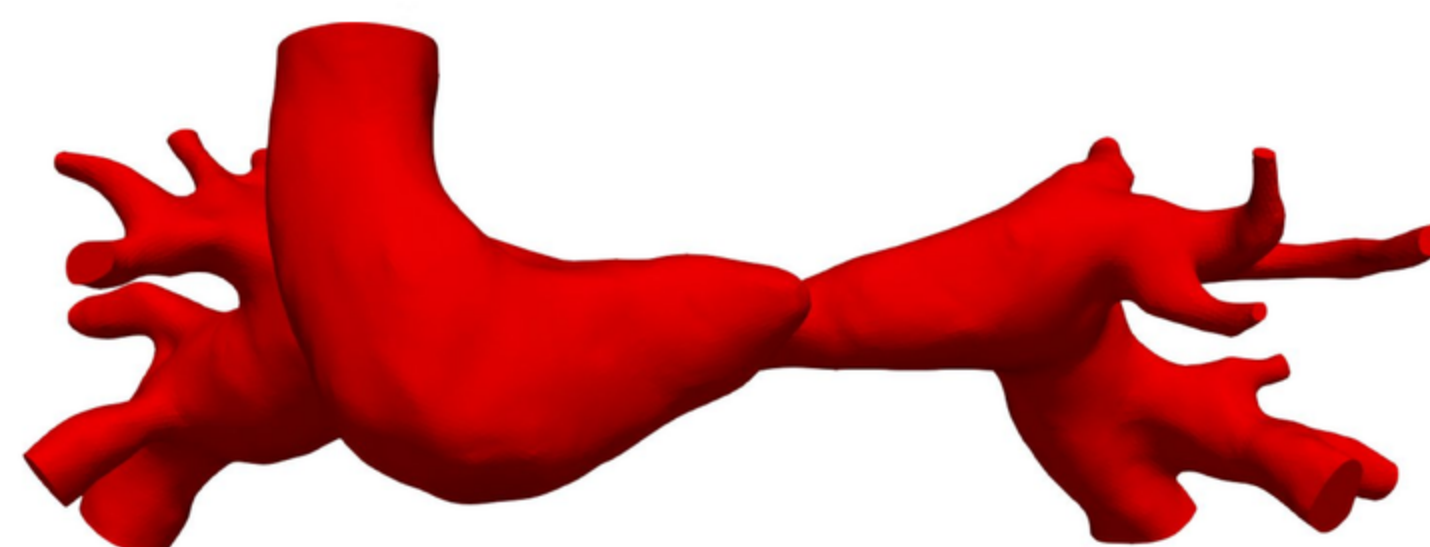
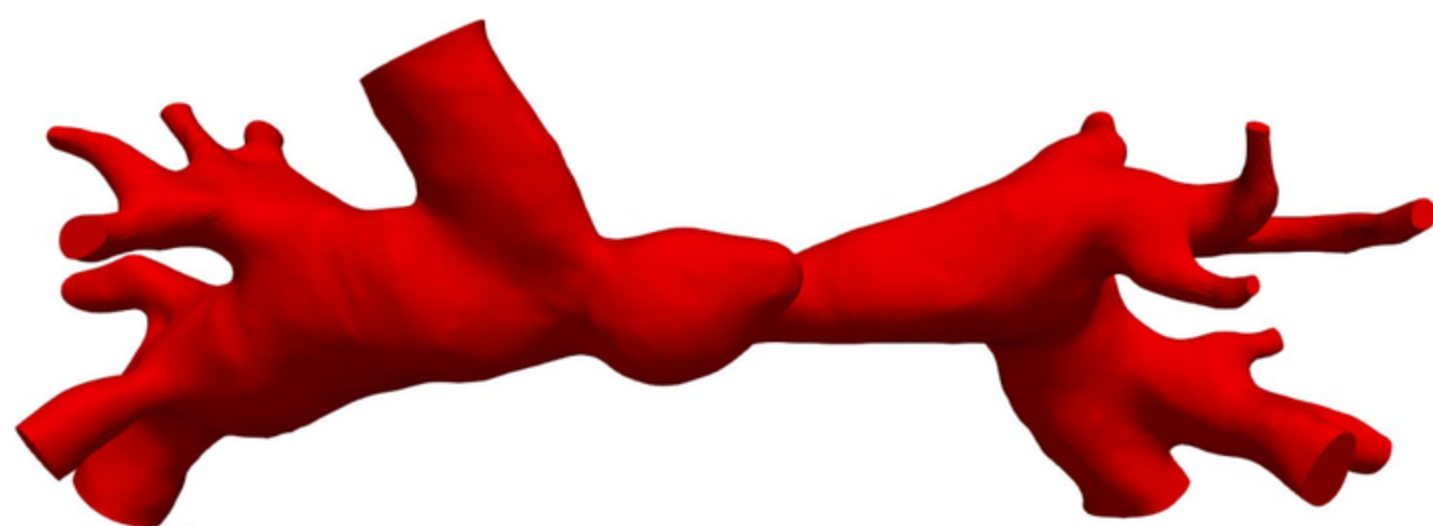
**Stage 1
reconstruction**



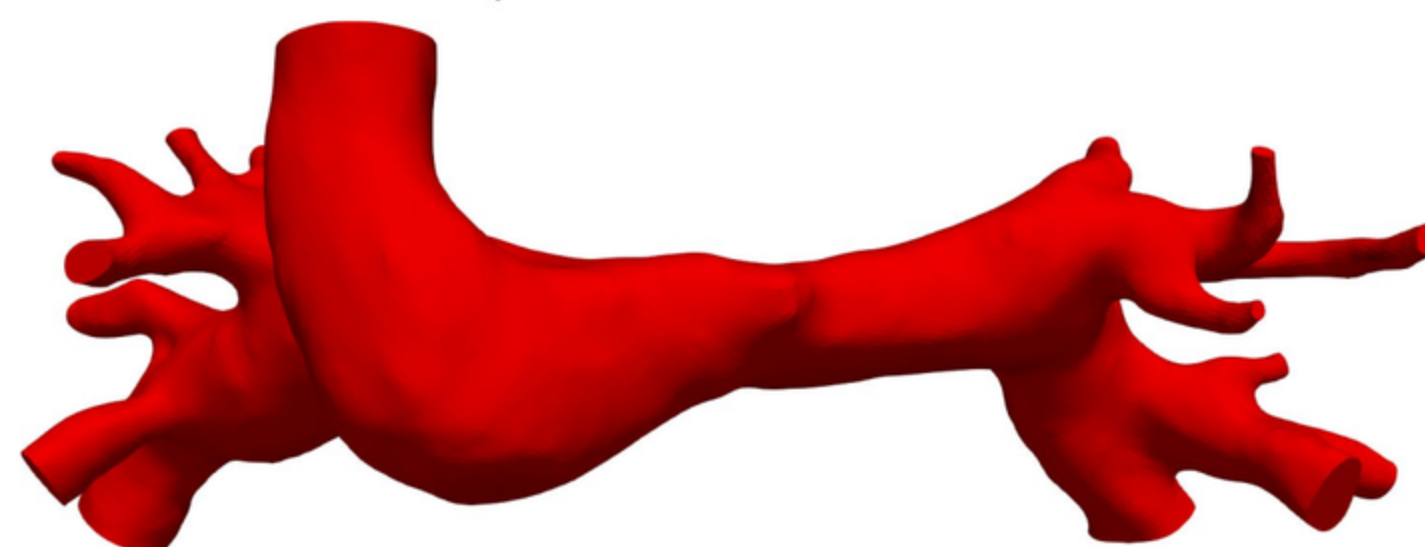
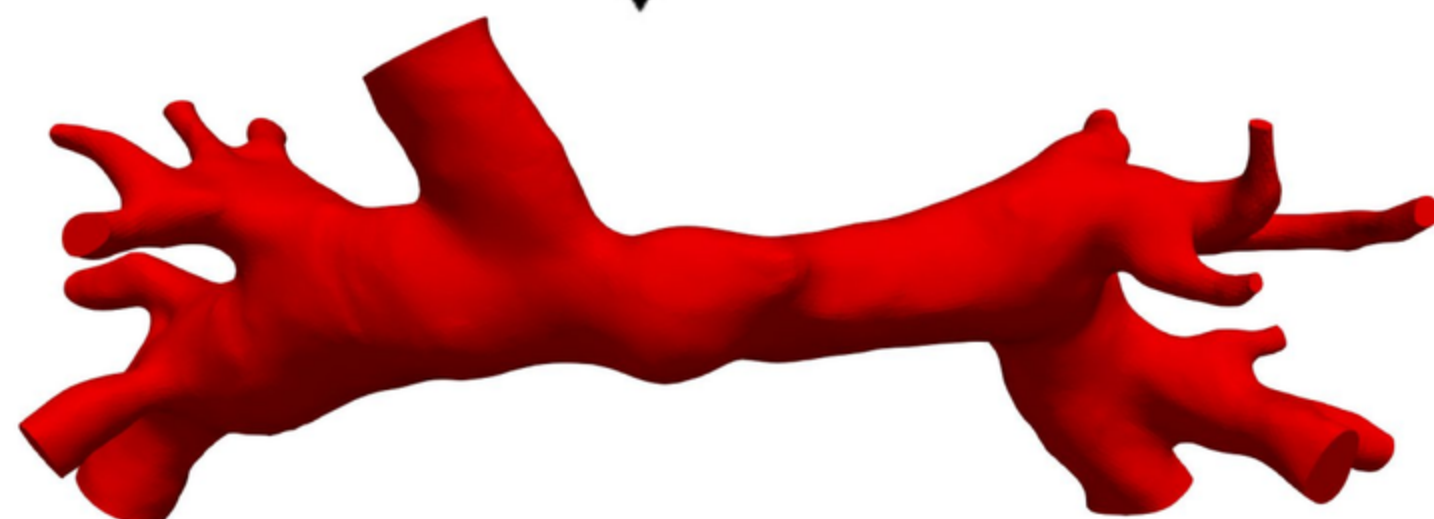
bG

hF

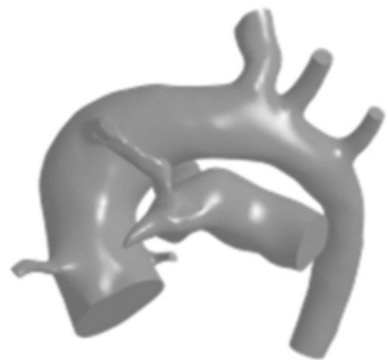
Stage 2



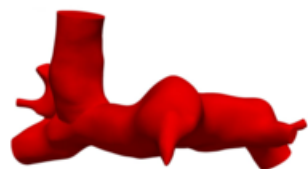
**with PA patch
plasty**



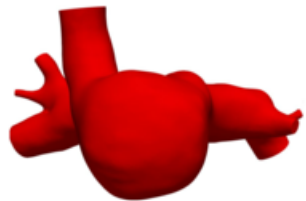
Patient A



bG



hF



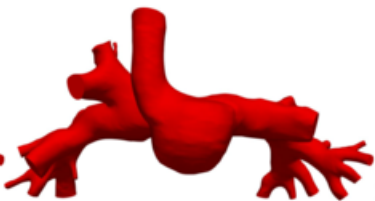
Patient C



bG



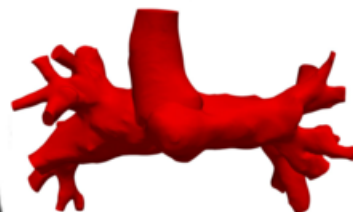
hF



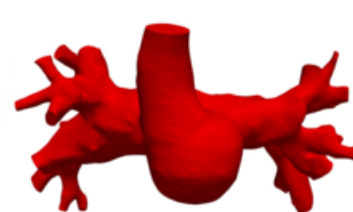
Patient E



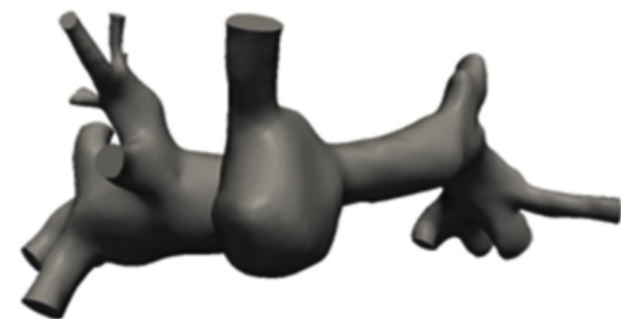
bG



hF



Patient F



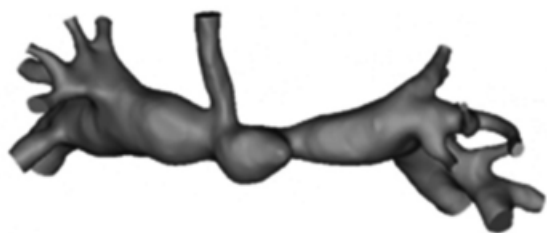
bG



hF



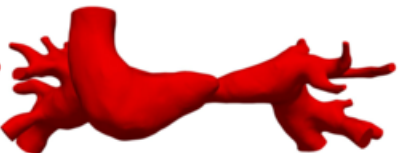
Patient B



bG



hF



bG with PA plasty hF with PA plasty



Patient D



bG



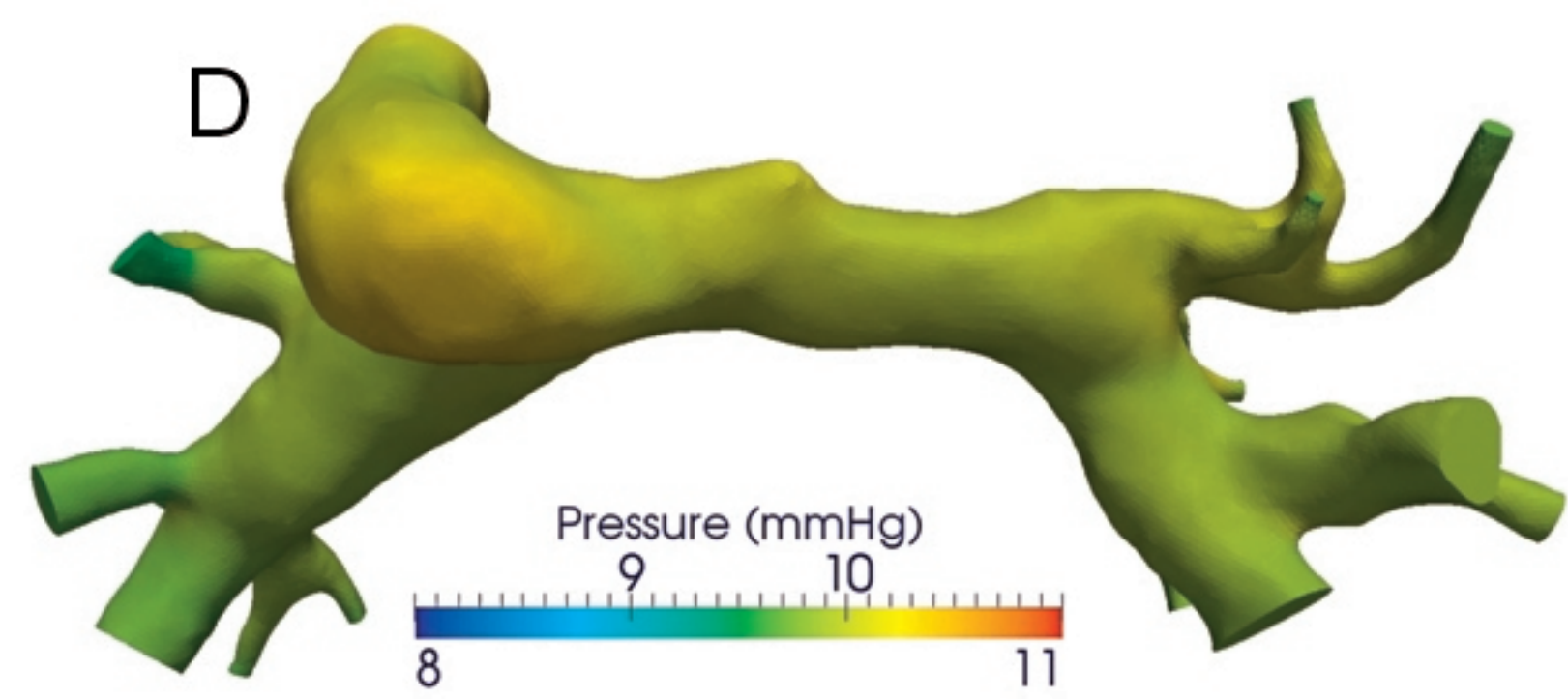
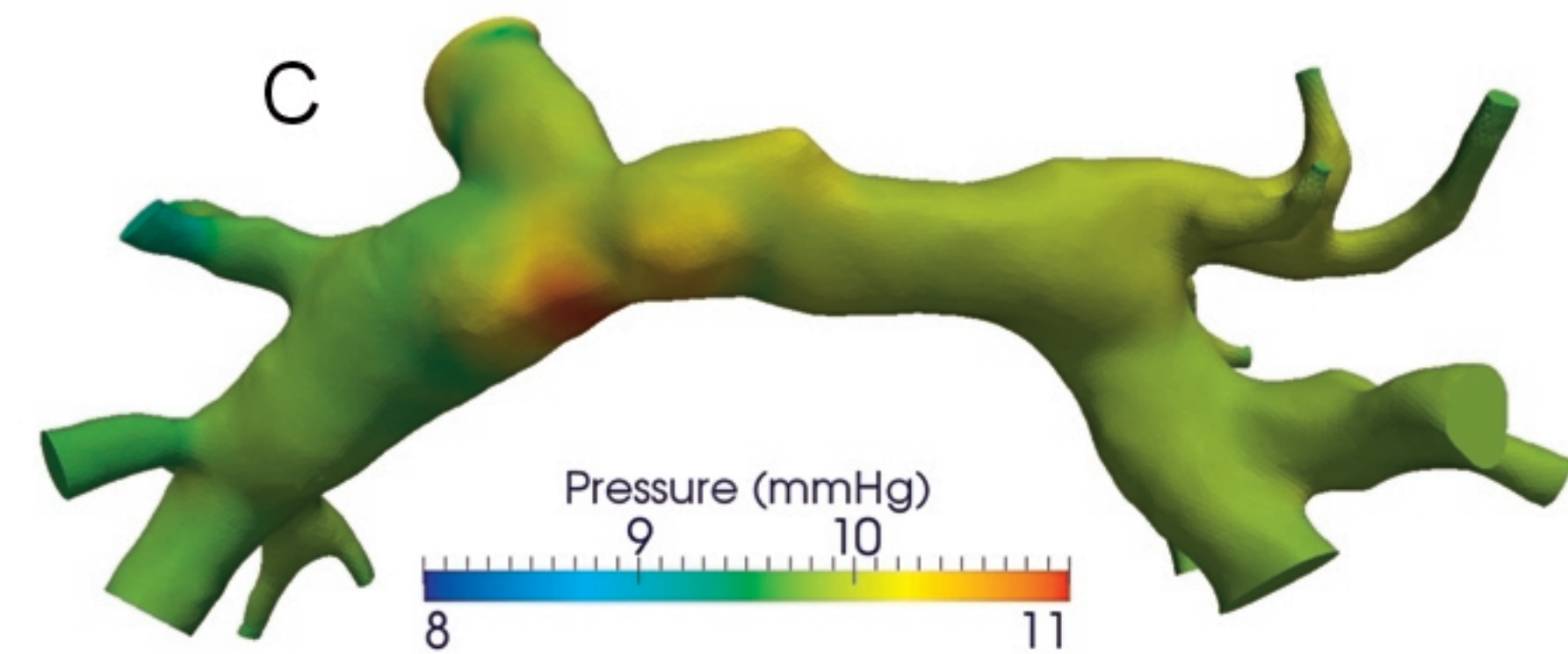
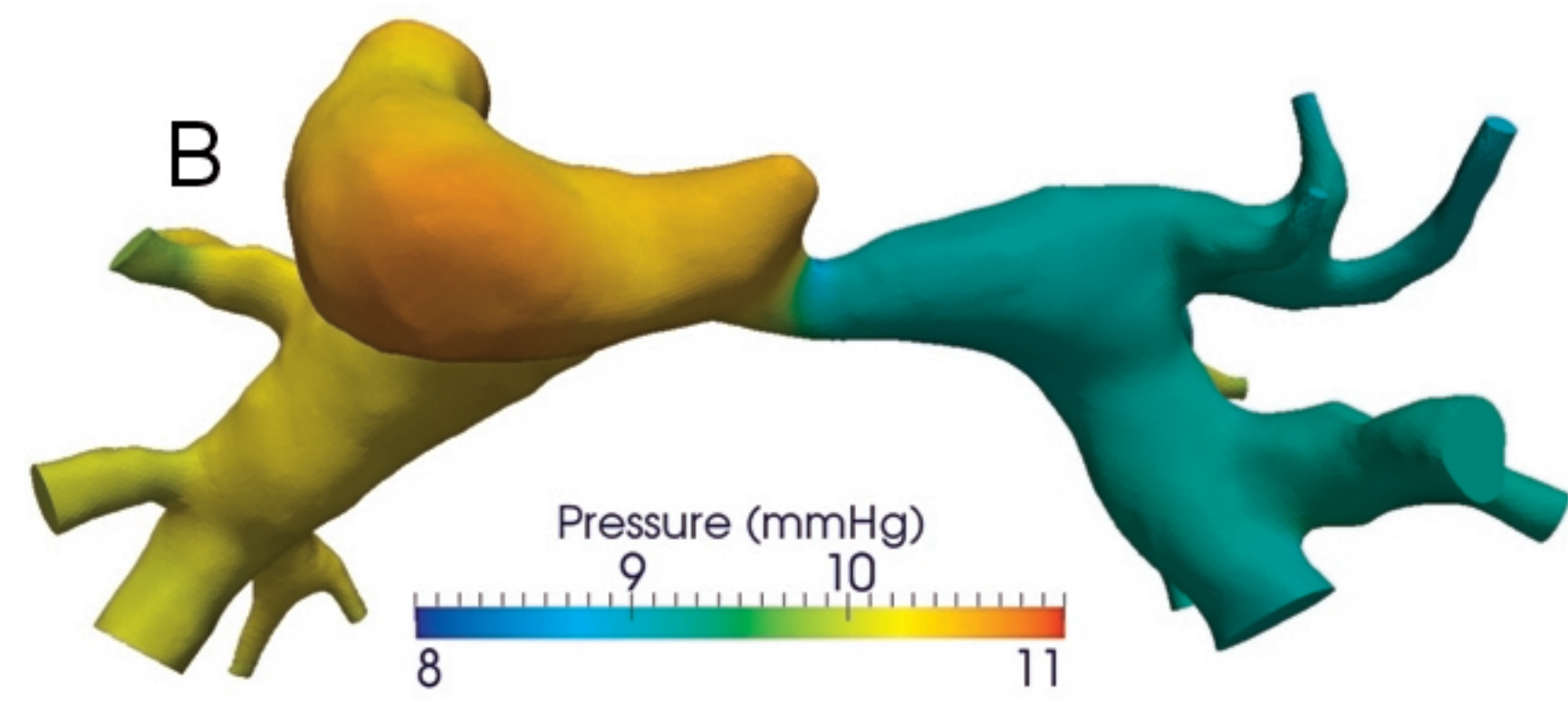
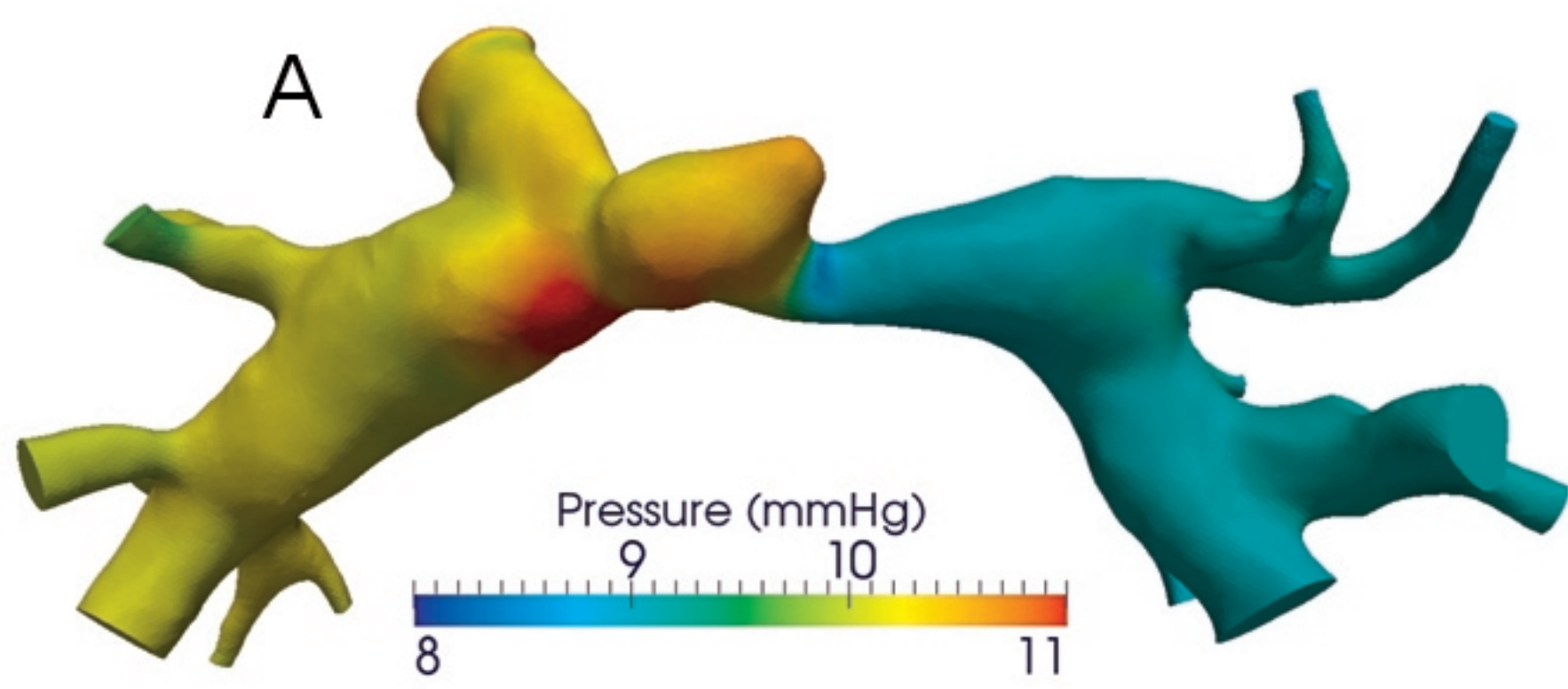
hF



bG with PA plasty hF with PA plasty



Pressure



Velocity

